The F-BAR domains from srGAP1, srGAP2 and srGAP3 regulate membrane deformation differently

Jaeda Coutinho-Budd[1], Vladimir Ghukasyan[2], Mark J. Zylka[1,2] and Franck Polleux[3,*]

[1]Neurobiology Curriculum University of North Carolina, Chapel Hill, NC 27599-7250, USA
[2]Neuroscience Center, University of North Carolina, Chapel Hill, NC 27599-7250, USA
[3]The Scripps Research Institute- Dorris Neuroscience Center, Department of Cell Biology, La Jolla, CA 92037-1000, USA
*Author for correspondence (polleux@scripps.edu)

Accepted 5 March 2012
Journal of Cell Science 125, 3390–3401
© 2012. Published by The Company of Biologists Ltd
doi: 10.1242/jcs.098962

Summary

Coordination of membrane deformation and cytoskeletal dynamics lies at the heart of many biological processes critical for cell polarity, motility and morphogenesis. We have recently shown that Slit-Robo GTPase-activating protein 2 (srGAP2) regulates neuronal morphogenesis through the ability of its F-BAR domain to regulate membrane deformation and induce filopodia formation. Here, we demonstrate that the F-BAR domains of two closely related family members, srGAP1 and srGAP3 [designated F-BAR(1) and F-BAR(3), respectively] display significantly different membrane deformation properties in non-neuronal COS7 cells and in cortical neurons. F-BAR(3) induces filopodia in both cell types, though less potently than F-BAR(2), whereas F-BAR(1) prevents filopodia formation in cortical neurons and reduces plasma membrane dynamics. These three F-BAR domains can heterodimerize, and they act synergistically towards filopodia induction in COS7 cells. As measured by fluorescence recovery after photobleaching, F-BAR(2) displays faster molecular dynamics than F-BAR(3) and F-BAR(1) at the plasma membrane, which correlates well with its increased potency to induce filopodia. We also show that the molecular dynamic properties of F-BAR(2) at the membrane are partially dependent on F-Actin. Interestingly, acute phosphatidylinositol 4,5-bisphosphate [PtdIns(4,5)P_2] depletion in cells does not interfere with plasma membrane localization of F-BAR(2), which is compatible with our result showing that F-BAR(2) binds to a broad range of negatively-charged phospholipids present at the plasma membrane, including phosphatidylserine (PtdSer). Overall, our results provide novel insights into the functional diversity of the membrane deformation properties of this subclass of F-BAR-domains required for cell morphogenesis.

Key words: F-BAR domain, srGAP, Membrane deformation, Filopodia

Introduction

The plasma membrane and actin cytoskeleton work in concert to create, maintain, and modify cell shape (Raucher et al., 2000; Sheetz and Dai, 1996). The coordination of plasma membrane deformation and actin polymerization is critical for cellular processes including chemotaxis, endocytosis, polarity and cytokinesis (Ford et al., 2002; Frost et al., 2007; Han et al., 2006; Janetopoulos et al., 2005; Martin-Belmonte et al., 2007; Vallis et al., 1999). The actin cytoskeleton can be linked to the plasma membrane through a diverse array of actin-binding proteins that interact directly with phosphoinositides, frequently phosphatidylinositol 4,5-bisphosphate [PtdIns(4,5)P_2], present in the inner leaflet of the plasma membrane, such as the Wiscott–Aldrich syndrome protein (WASP) family proteins (Miki et al., 1996; Oikawa et al., 2004), actin depolymerizing factor (ADF)/cofilins (Zhao et al., 2010) and the small Rho-like GTPases (Yoshida et al., 2009). Alternatively, this link to the actin cytoskeleton can occur through scaffolding proteins that contain specific phospholipid-binding motifs, such as pleckstrin homology (PH) domains found in proteins such as phospholipase C (PLC), dynamin (Flesch et al., 2005; Harlan et al., 1994; Vallis et al., 1999), or Bin/amphiphysin/Rvs (BAR)-domain-containing proteins (reviewed by Itoh and De Camilli, 2006; Tsujita et al., 2006). Over the past decade, emerging evidence suggests that in many instances F-actin dynamics is coupled to the function of membrane-deforming proteins. This coupling plays an instructive role in the localization and the type of membrane deformations observed in cells, such as lamellipodia and filopodia protrusions during endocytosis or phagocytosis (Doherty and McMahon, 2008; Itoh and De Camilli, 2006; Martin-Belmonte et al., 2007).

Proteins of the BAR superfamily are recognized for their ability to both sense and generate membrane curvature (Doherty and McMahon, 2008). BAR domains are membrane-binding modules, consisting of a series of three to five α-helices, that have a large dimerization interface to create banana-shaped quaternary structures. These homodimeric BAR domains bind cellular membranes through electrostatic charge interaction between their positively charged amino acids (arginine and lysine) and the negatively charged phospholipids of the membrane, such as PtdIns(4,5)P_2 and phosphatidylserine (PtdSer) (Saarikangas et al., 2009). BAR-domain-containing proteins often contain multiple other domains, including the actin-binding domain WH2, GTPase-activating protein (GAP) and guanine-nucleotide-exchange factor (GEF) domains, and Src homology 3 (SH3) domains, leading to the interplay between cellular membranes and the actin cytoskeleton. The BAR superfamily has been segregated into subfamilies, based on structural and functional data (Itoh and De Camilli, 2006). N-BAR domains, such as those found in amphiphysin and

Journal of Cell Science

endophilin, contain a N-terminal amphipathic helix that inserts into the lipid bilayer, aiding in their membrane-deforming properties (Masuda et al., 2006; Peter et al., 2004). BAR domains induce membrane invaginations, and function in endocytosis. F-BAR domains were recognized more recently through secondary structure prediction of the congruence of a Fes-CIP4 homology (FCH) domain and a coiled-coil domain in its C-terminal (Henne et al., 2007; Itoh et al., 2005; Shimada et al., 2007; Tsujita et al., 2006). Recently, several structures of F-BAR domains have been solved, revealing that these have an elongated dimer structure with more shallow curvature than the BAR domains (Shimada et al., 2007; Wang et al., 2009; Yoshida et al., 2009). Like BAR proteins, F-BAR-domain-containing proteins, such as formin-binding protein 17 (FBP17) and FCH only 1 and 2 (FCHO1/2) induce membrane invaginations and play a role in the endocytic process (reviewed by Doherty and McMahon, 2008). A third class of protein, inverse BAR (I-BAR)-domain-containing proteins such as insulin receptor tyrosine kinase substrate p53 (IRSp53) and missing-in-metastasis (MIM) induce membrane protrusions instead of invaginations (Mattila et al., 2007; Suetsugu et al., 2006; Yamagishi et al., 2004). However, this simple structure/function dichotomy, whereby N-BAR, F-BAR and BAR domains induce membrane invagination and tubulation, whereas I-BAR domains induce filopodial protrusions, has been recently challenged by results showing that the predicted F-BAR domain of Slit-Robo GTPase activation protein 2 (srGAP2) (Guerrier et al., 2009) and syndapins (Dharmalingam et al., 2009) can induce filopodia-like membrane protrusion and, thereby, regulate neuronal morphogenesis.

srGAP2 is a member of the srGAP family of proteins, which consists of three other members: srGAP1, srGAP3 (also known as WRP and Megap) and ArhGAP4 (which has been renamed srGAP4 based on its domain organization and homology with srGAP1–3; MGI 2159577). srGAP proteins all contain a predicted N-terminal F-BAR domain, a central Rho-GAP domain and a C-terminal SH3 domain (Carlson et al., 2011; Wong et al., 2001). The family was named based on the fact that the C-terminal SH3 domain binds the intracellular domain of the Roundabout receptor (Robo), the receptor for the axon guidance cue, Slit (Wong et al., 2001). Although each family member contains a GAP domain, there are differences in GTPase hydrolysis activity between the proteins. The RhoGAP domain of srGAP1 has been shown to promote GTP hydrolysis of Cdc42 and RhoA, depending on the concentration of Slit1 (Wong et al., 2001), whereas the GAP domains of srGAP2 and srGAP3 are both specific for Rac1 (Guerrier et al., 2009; Soderling et al., 2002), and ArhGAP4 can act on both Cdc42 and Rac1 (Vogt et al., 2007). All four family members display spatially and temporally distinct patterns of expression in the central nervous system (Bacon et al., 2009; Foletta et al., 2002) and have been shown to regulate cell migration and neuronal morphology in mammalian cells (Guerrier et al., 2009; Soderling et al., 2002; Vogt et al., 2007; Wong et al., 2001; Yang et al., 2006), a function that seems evolutionary conserved in invertebrates (Zaidel-Bar et al., 2010). srGAP3 has been implicated in a severe form of mental retardation, the 3p− syndrome, giving srGAP3 the alternate name of mental-disorder associated GAP protein (MEGAP) (Endris et al., 2002). srGAP2 has also recently been implicated in a severe neurodevelopmental syndrome causing early infantile epileptic encephalopathy and profound psychomotor delay (Saitsu et al., 2011). These human genetic data strongly suggest that srGAP2 and srGAP3 play a crucial role during human brain development.

We recently found that the function of srGAP2 in both neuronal migration and morphogenesis is largely mediated through the ability of its F-BAR domain to induce filopodia (Guerrier et al., 2009). However, the functional properties of the predicted F-BAR domains of the remaining srGAP family members have yet to be determined; furthermore, the molecular mechanisms underlying their function during filopodia formation are only starting to be examined in detail (Carlson and Soderling, 2009).

In the present study, we focused our analysis on the function of the F-BAR domains present in srGAP1, srGAP2 and srGAP3. Our results reveal a surprising degree of diversity in the ability of these three closely related F-BAR domains to induce filopodia-like membrane protrusions in non-neuronal and neuronal cells. Our study provides novel insights into the molecular mechanisms underlying the membrane deformation properties of this subclass of F-BAR domains during cell morphogenesis.

Results

The srGAP family of proteins, through their respective F-BAR domains, exhibit differing abilities to induce filopodia in non-neuronal cells

Recently, the F-BAR domain of srGAP2 [designated F-BAR(2)] has been implicated in the regulation of neuronal migration and morphogenesis owing to its ability to induce filopodia and neurite branching (Guerrier et al., 2009). srGAP2 is one of four srGAP family proteins, although ArhGAP4/srGAP4 diverges in sequence from the rest of the family (supplementary material Fig. S1A,B); therefore, we restricted our analysis to the F-BAR domains of srGAP1, srGAP2 and srGAP3. Although the F-BAR domains of srGAP1, srGAP2 and srGAP3 share ~85% amino-acid identity (supplementary material Fig. S1C,D), the molecular properties of the F-BAR domains of srGAP1 and srGAP3 [designated F-BAR(1) and F-BAR(3), respectively] are still poorly understood. To first compare the functions of these closely related proteins, we transfected plasmids expressing full-length srGAPs, or their respective F-BAR domains, fused at their C-terminal end to enhanced green fluorescent protein (EGFP), into COS7 cells (Fig. 1A–H″). Full-length srGAP1 (Fig. 1B–B″,I,J) and srGAP3 (Fig. 1D–D″,I,J) induce more filopodia than EGFP alone (Fig. 1A–A″,I,J), but are both significantly less potent than full-length srGAP2 (Fig. 1C–C″,I,J). A similar trend is found with expression of each respective F-BAR domain (Fig. 1E–G″). Therefore, both srGAP2 and its F-BAR(2) domain are more potent at inducing filopodia than srGAP3 and srGAP1, or their F-BAR domains (Fig. 1I,J). Additionally, both srGAP2 and F-BAR(2) induced significantly longer filopodia than the other srGAP family members or their F-BAR domains (Fig. 1K). There is no significant difference in filopodia number or length between each srGAP protein and its respective F-BAR domain. These data illustrate that despite such closely related sequences, the members of the srGAP family of proteins are functionally distinct with regard to their ability to induce filopodia.

srGAP proteins can interact through their F-BAR domains

It has previously been shown that BAR, N-BAR, F-BAR and I-BAR domains homodimerize to form curved structures necessary for membrane deformation and tubulation (Henne et al., 2007; Shimada et al., 2007; Wang et al., 2009; Frost et al., 2008). We

Journal of Cell Science

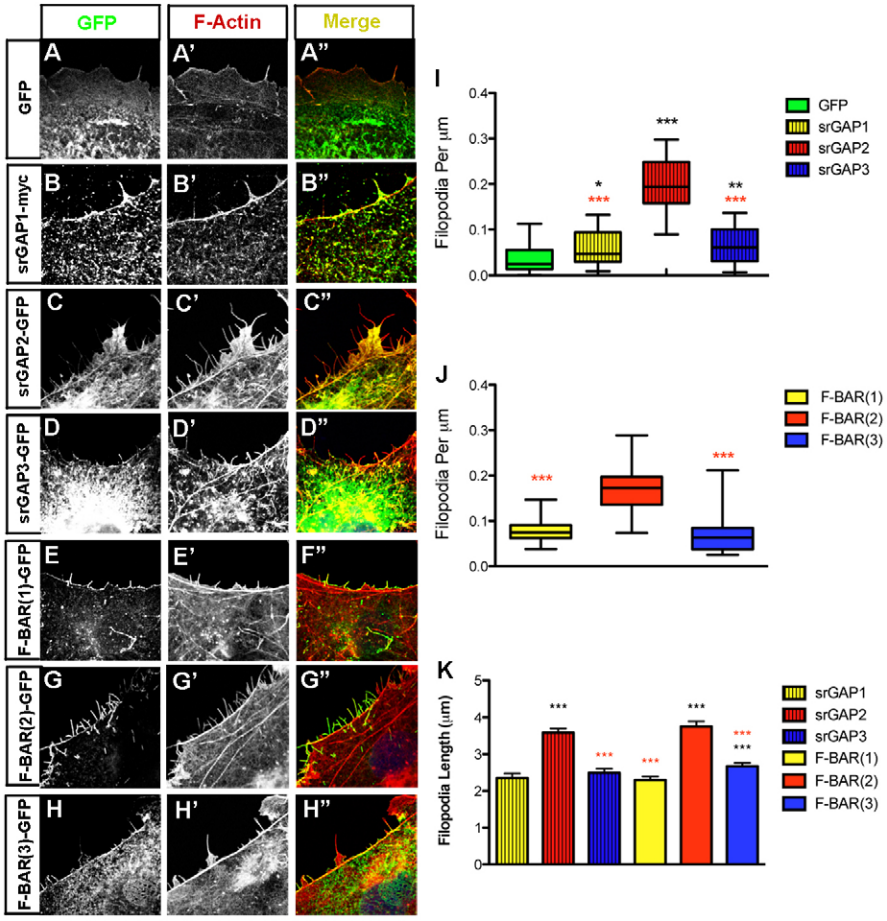

Fig. 1. srGAP2 induces significantly more filopodia than srGAP1 or srGAP3. (**A–H″**) COS7 cells expressing EGFP only (A′–A″), EGFP-tagged full-length srGAP1 (B–B″), srGAP2 (C–C″) or srGAP3 (D–D″), or their respective F-BAR domains (E–H″) were counterstained with phalloidin for F-actin (A′–H′) in red. (**I–J**) Quantification of the effects described in A–H″ (n>25 cells). (K) srGAP2 and its F-BAR domain [F-BAR(2)] induce significantly longer filopodia than full-length srGAP1, srGAP3, or their respective F-BAR domains (n>200 filopodia; P<0.0001). Quantifications were taken from at least three independent experiments and analyzed using a non-parametric Mann–Whitney test. *P<0.05 (0.0193), **P<0.01 (0.0068), ***P<0.001; black asterisks indicate comparison with EGFP and red asterisks indicate comparison with srGAP2–EGFP or F-BAR(2)–EGFP.

have previously shown, using biochemical and biophysical approaches, that the F-BAR domain of srGAP2 forms homodimers (Guerrier et al., 2009). Based on their high degree of conservation, we hypothesized that the F-BAR domains of the srGAP family proteins have the ability to heterodimerize as well as homodimerize. To test for interaction between F-BAR domains, combinations of myc-tagged and GFP-tagged srGAPs were co-transfected into COS7 cells and immunoprecipitated with an anti-GFP antibody (Fig. 2A). Western blots were probed for myc, revealing interactions between all three paired combinations of full-length srGAP proteins. This interaction occurred through the respective F-BAR domains, and not through indirect interaction through SH3 domain binding, as indicated by co-immunoprecipitation of RFP-tagged F-BAR(2) with GFP-tagged F-BAR(1)/(3) (Fig. 2B). This result suggests that all three F-BAR domains are structurally conserved and are capable of heterodimerization or oligomerization.

The F-BAR domains of different srGAP proteins localize to distinct regions of filopodia

In order to test for cooperative function of these three different F-BAR domains, GFP-tagged F-BAR(1) or F-BAR(3) were co-transfected into COS7 cells along with mRFP-tagged F-BAR(2) (Fig. 3A–C″). Surprisingly, co-expression of either F-BAR(1) (Fig. 3A–A″) or F-BAR(3) (Fig. 3C–C″) with F-BAR(2) led to a synergistic effect towards filopodia induction when compared with the equivalent expression of F-BAR(2)–GFP and F-BAR(2)–mRFP (Fig. 3B–B″; quantified in Fig. 3D). Live-imaging of co-transfected COS7 cells revealed differences in filopodial dynamics in cells expressing different F-BAR combinations: filopodia containing GFP- and RFP-tagged F-BAR(2) or the combination of F-BAR(2)–RFP and F-BAR(3)–GFP extended faster than filopodia containing F-BAR(2)–RFP and F-BAR(1)–GFP (Fig. 3E).

We noticed that when co-expressed, these F-BAR domains had a distinct distribution along the filopodia. In order to quantify F-BAR distribution within the filopodia of COS7 cells, a line was drawn from the base to the tip of the filopodia to measure the fluorescence intensity of both the GFP- and mRFP-tagged signals. This quantification reveals significant differences in F-BAR distribution into the filopodia (Fig. 3F–H, quantified in Fig. 3I). In both instances, F-BAR(2) extended to the tip of the filopodia, whereas the expression of F-BAR(1) or F-BAR(3) strongly decreased before reaching the tip. These results suggest (1) that the F-BAR domains of srGAP1–3 display synergistic effects towards filopodia induction and filopodia growth, and (2) that these three F-BAR domains have distinct intra-filopodial localization when co-expressed. These data, combined with the interaction data, further suggest that the three F-BAR domains can form distinct complexes inside a filopodium to intricately regulate the induction and maintenance of membrane protrusions.

Molecular dynamics of the F-BAR domains of srGAP1-3

Canonical F-BAR domain homodimers can form end-to-end oligomers that adopt a ‘coiled’ quaternary structure, which interacts with the plasma membrane (Shimada et al., 2007).

Journal of Cell Science

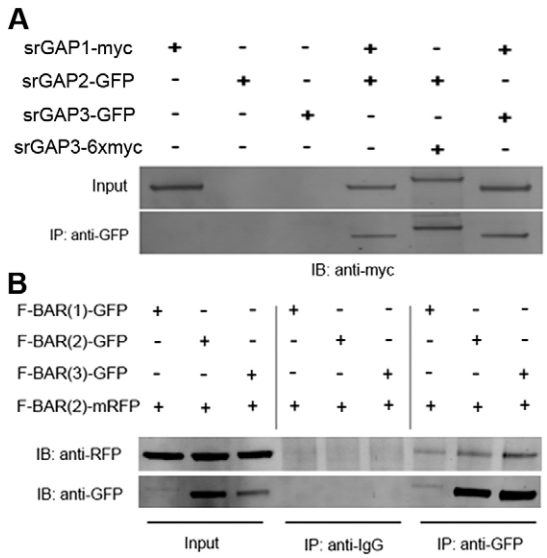

Fig. 2. srGAP proteins interact through their F-BAR domains. (**A**) Combinations of EGFP- and myc-tagged full-length srGAP proteins were coexpressed in COS7 cells, immunoprecipiated (IP) with anti-GFP and immunoblotted (IB) with anti-myc antibodies. Single-transfected control lysates demonstrate the specificity of the rabbit anti-EGFP and mouse anti-myc antibodies. Every combination of the three srGAP proteins was able to co-immunoprecipitate. (**B**) EGFP-tagged F-BAR(1)–F-BAR(3) were coexpressed with mRFP-tagged F-BAR(2) in COS7 cells. Cells lysates were incubated and immunoprecipitated with either rabbit anti-IgG control antibody or rabbit anti-EGFP antibody, and immunoblotted for either rabbit anti-RFP antibody or mouse anti-GFP antibody. All three EGFP-tagged F-BAR domains co-immunoprecipitated with F-BAR(2)–mRFP.

These 'coils' are also stabilized by interactions between the sides of the F-BAR homodimers occurring between adjacent turns of the 'coil' in proteins such as FBP17 (Frost et al., 2008). The exact structural mechanism underlying I-BAR-mediated membrane tubulation in filopodia is currently unknown, but has been shown to require the ability of I-BAR domains to interact with the negatively-charged lipids via the convex surface, as well as insertion of an amphipathic helix into the inner leaflet of the plasma membrane (Saarikangas et al., 2009). Additionally, the I-BAR domains of IRSp53 (Millard et al., 2005), IRTKS (Millard et al., 2007) and MIM (Lee et al., 2007) have been suggested to directly bind to actin. We hypothesized that part of the functional differences observed between the ability of the three srGAP F-BAR domains to induce filopodia might be due to differences in their subcellular trafficking properties along the plasma membrane or the actin cytoskeleton, which can be assessed by quantifying their molecular dynamics using fluorescence recovery after photobleaching (FRAP).

Following photobleaching, the fluorescence recovery (F_R) plateaus at a certain percentage of the initial fluorescence, which represents the fraction of the protein that is mobile (mobile fraction). We also measured the time required to recover 50% of the fluorescence of the mobile fraction ($t_{1/2}$), which indicates the speed of the mobile fraction (i.e. how quickly F-BAR domains assemble and traffic along the plasma membrane). We made three types of comparisons for both F_R and $t_{1/2}$: (1) comparing all three F-BAR domains and the PH domain of PLCδ1, (2) comparing the molecular dynamics of these domains in filopodia versus along the plasma membrane, and (3) comparing the molecular dynamics of these domains in control cells versus cells treated with cytochalasin D in order to induce F-actin depolymerization (supplementary material Fig. S2).

These quantitative analyses reveal that F-BAR(2) displays a significantly higher mobile fraction and shorter $t_{1/2}$ than F-BAR(1), in filopodia (Fig. 4B,C) and at the plasma membrane (Fig. 4D,E), whereas F-BAR(3) can behave in a similar manner to both of the other F-BAR domains, depending on the context. In filopodia, the mobile fraction of F-BAR(3) matches that of F-BAR(2) in untreated cells, whereas the mobile fraction of F-BAR(3) matches that of F-BAR(1) at the peripheral membrane; however, depolymerization of the actin cytoskeleton with cytochalasin D reduces the mobile fraction coefficient of F-BAR(3) to that of F-BAR(1) in filopodia, and raises the mobile fraction coefficient of F-BAR(3) at the membrane. Additionally, these experiments revealed that the speed of F-BAR mobility relies on an intact F-actin cytoskeleton, given that depolymerization of F-actin by cytochalasin D treatment significantly increased $t_{1/2}$ for all three F-BAR domains, both in filopodia and at the plasma membrane (Fig. 4C,E). Given the direct interaction of actin with the plasma membrane (Raucher et al., 2000), it is possible that the effects of cytochalasin D treatment on F-BAR domain mobility at the membrane are due to indirect effects on lipid diffusion rates. To rule out this possibility, we performed the same FRAP experiments with the PH domain of PLCδ1, which specifically binds PtdIns(4,5)P_2. This analysis revealed two interesting differences in the molecular dynamics of F-BAR and PH domains. First, the PH domain displays significantly faster molecular dynamics (both increased mobile fraction and decreased $t_{1/2}$). Second, cytochalasin-D-mediated actin depolymerization did not affect the mobile fraction coefficient or the $t_{1/2}$ of the PH domain either inside filopodia or at the plasma membrane (Fig. 4). These results reveal two important new features regarding the molecular dynamics of these F-BAR domains in filopodia: (1) the molecular dynamics correlate well with the efficiency of each F-BAR domain to induce filopodia [i.e. F-BAR(2)>F-BAR(3)>F-BAR(1)], and (2) the rate of intracellular mobility of the F-BAR domains is partially dependent on F-actin.

Lipid specificity varies between the F-BARs of srGAP proteins

All BAR-like domains, including F-BAR and I-BAR domains, bind to the plasma membrane through electrostatic interactions to negatively charged phospholipids, such as PtdIns(4,5)P_2 (Itoh et al., 2005; Mattila et al., 2007; Peter et al., 2004; Saarikangas et al., 2009), and/or through the presence of an amphipatic helix (wedge loop) directly inserting into the phospholipid bilayer (Saarikangas et al., 2009; Wang et al., 2009). Membrane-binding proteins can be removed from the membrane in a variety of ways, such as exposure to salt solutions (e.g. weaker interactions can be disrupted by lower salt concentrations). Different lipid compositions can also be separated using different detergent solutions (London and Brown, 2000). Western blots of lysates from cells expressing F-BAR(1), F-BAR(2) and F-BAR(3) would reveal any differing affinities for Triton-X-insoluble lipids and proteins. To test this, cells were lysed in a two-step process, first with a low-stringency Triton-X-containing buffer, then the supernatant was removed, and the insoluble pellet was subjected to a higher-stringency modified RIPA buffer and sonicated. Molecular components of the Triton-X-insoluble

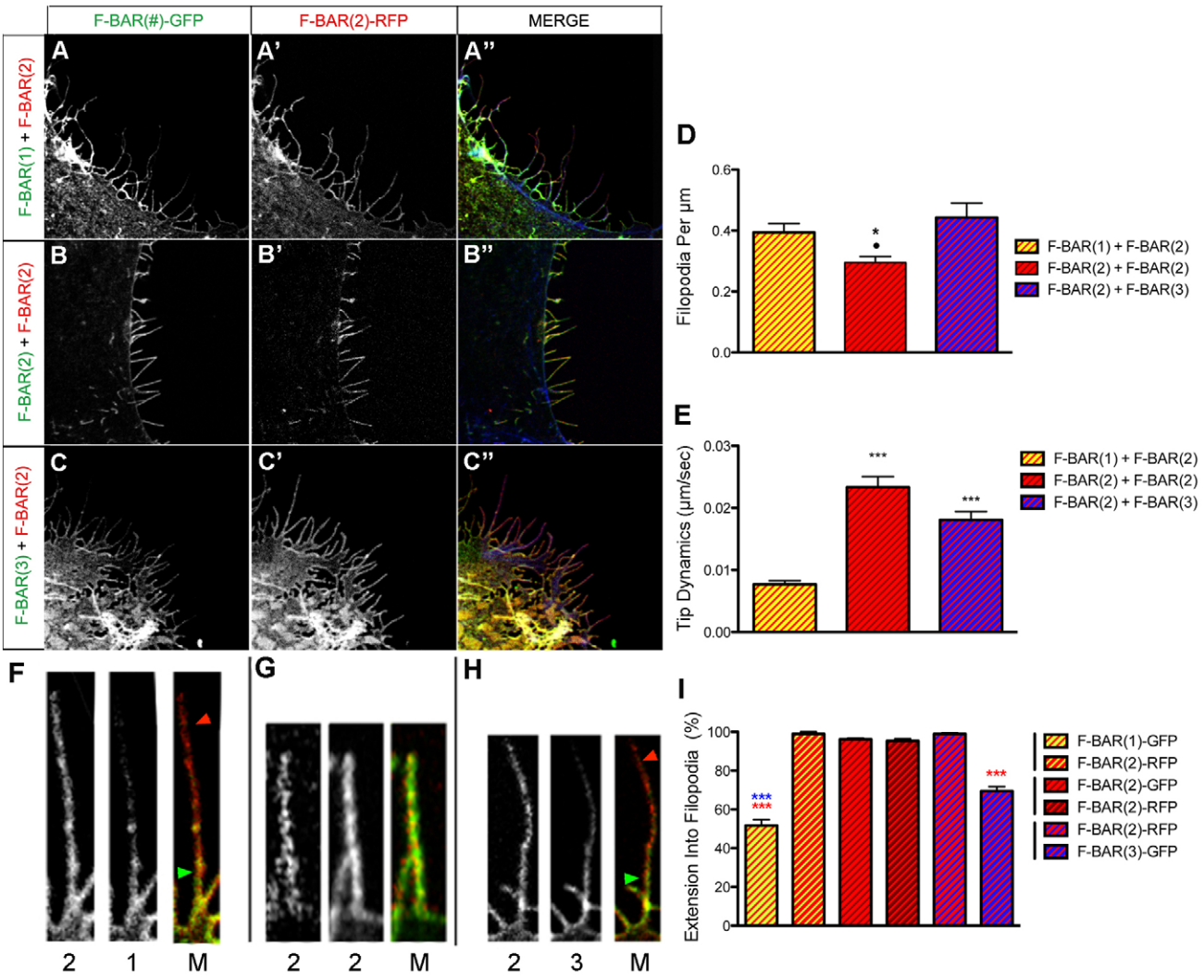

Fig. 3. Synergy between F-BAR domains towards filopodia induction. (**A**–**C″**) Coexpression of F-BAR(1)–GFP and F-BAR(2)–mRFP (A–A″), F-BAR(2)–GFP and F-BAR(2)–mRFP (B–B″), and FBAR(2)–mRFP and F-BAR(3)–GFP (C–C″) in COS7 cells. (**D**) Quantification of filopodia density in F-BAR-transfected COS7 cells. Co-transfection of F-BAR(1)–GFP or F-BAR(3)–GFP with F-BAR(2)–mRFP do not differ in their filopodia densities; however, both combinations induce significantly higher filopodia densities than any single F-BAR alone [$n>25$ cells; * and • indicate $P<0.005$, with * depicting significance between F-BAR(1) and F-BAR(2), and • marking significance between F-BAR(2) and F-BAR(3)]. (**E**) Quantification of filopodial dynamics based on the path travelled by the filopodia tips ($n>186$ filopodia; ***$P<0.0001$). (**F–I**) Intrafilopodia expression of each F-BAR varies in co-transfected COS7 cells, whereas F-BAR(1)–GFP extinguishes before F-BAR(2)–RFP (F), F-BAR(2)–GFP and F-BAR(2)–RFP both extend to the filopodial tip (G), and F-BAR(2)–RFP extends beyond F-BAR(3)–GFP (H); quantified in (I). $n=50$ for F-BAR(1) and F-BAR(2); $n=75$ for F-BAR(2) and F-BAR(2); $n=83$ for F-BAR(2) and F-BAR(3); ***$P<0.0001$, red asterisks indicate comparison with F-BAR(2), and blue asterisks indicate comparison with F-BAR(3). Quantifications were taken from at least three independent experiments and analyzed using a Mann–Whitney non-parametric test.

fraction contain lipids found in lipid rafts, which are highly enriched for cholesterols and sphingolipids (London and Brown, 2000), as well as phosphatidylethanolamine (PtdEth), phosphatidylcholine (PtdChl), phosphatidylserine (PtdSer) and phosphatidylinositol (PtdIns) (Rouquette-Jazdanian et al., 2002). F-BAR(1) and F-BAR(3) have a 32-fold and 7.4-fold higher affinity for the Triton-X-insoluble fraction, respectively, whereas F-BAR(2) is only present at 0.6-fold that found in the Triton-X-soluble fraction (Fig. 5A).

Recently, Carlson and colleagues have reported that F-BAR(3) relies on PtdIns(4,5)P_2 for its membrane binding (Carlson et al., 2011). Membrane localization was reduced with the coexpression of the PtdIns(4,5)P_2-specific 5-phosphatase, Inp54p; however, constitutive Inp54p expression has been shown to negatively effect cell morphology and health, causing cell rounding and a loss of protrusions (Raucher et al., 2000). Although recombinant F-BAR(2) domain binds PtdIns(4,5)P_2, it also binds several negatively charged phosphoinositides, as well as PtdSer (Fig. 5B; supplementary material Fig. S3).

Given the high degree of similarity between F-BAR(2) and F-BAR(3), and that PtdIns(4,5)P_2 is the most abundant form of phosphorylated PtdIns at the plasma membrane of many mammalian cells (Mitchell et al., 1986; Tran et al., 1993), we next tested whether PtdIns(4,5)P_2 is required for the maintenance of F-BAR localization at the plasma membrane in situ by employing an acute rapamycin-inducible method of depleting

Journal of Cell Science

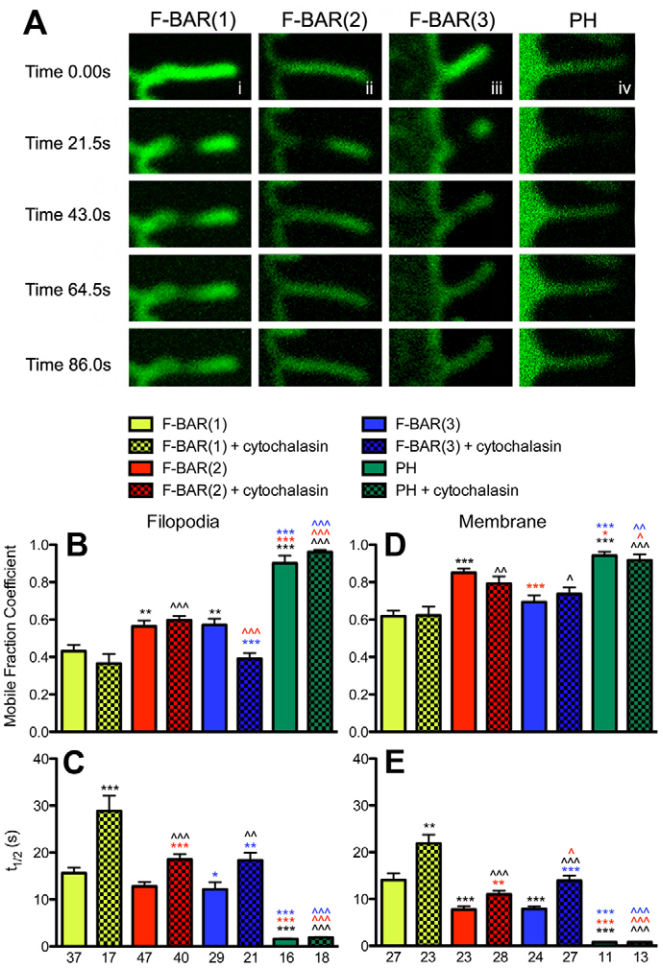

Fig. 4. The three F-BAR domains of srGAP proteins differ in their subcellular molecular dynamics. (**A**) FRAP analysis of EGFP-tagged F-BAR(1) (i), F-BAR(2) (ii), F-BAR(3) (iii), and PH domain of PLCδ1 (iv) in filopodia protrusions. The same analyses were performed at the peripheral membrane of the cell. (**B**–**E**) Quantification of the mobile fraction coefficient (B,D) and half-time of recovery ($t_{1/2}$; C,E) in filopodial protrusions (B–C) and at the peripheral plasma membrane (D–E). Cells were either imaged as untreated controls, or treated with cytochalasin-D for depolymerization of the actin cytoskeleton. Significance compared to untreated controls are marked by asterisks (*), and significance to cytochalasin-treated samples is marked with a caret (^). Significance is color-coded with black for F-BAR(1), red for F-BAR(2) and blue for F-BAR(3). *n* for each condition is marked below the bottom graph for filopodial and membrane, and is the same for mobile fraction and $t_{1/2}$ at each location. $^{*/\wedge}P<0.05$, $^{**/\wedge\wedge}P<0.005$, $^{***/\wedge\wedge\wedge}P<0.0005$.

PtdIns(4,5)P_2 from the membrane (Varnai et al., 2006). This method allows for temporal control of PtdIns(4,5)P_2 depletion and can avoid some of the consequences of constitutive PtdIns(4,5)P_2 depletion (Raucher et al., 2000). Briefly, addition of rapamycin induces binding of the membrane-targeted FKBP-rapamycin-binding (FRB) domain to the FK506-binding protein (FKBP) domain, thereby recruiting Venus-FKBP-Inp54p, a PtdIns(4,5)P2-specific 5-phosphatase, to the plasma membrane where it dephosphorylates PtdIns(4,5)P_2 into PtdIns(4)*P* (Varnai et al., 2006) (Fig. 5C–U). Prior to rapamycin treatment, the FRB domain (Fig. 5D,J,P) and PH domain of PLDδ1 (Fig. 5F), F-BAR(2) (Fig. 5L) and F-BAR(3) (Fig. 5R) are localized to the plasma membrane, while the FKBP12-Inp54p fusion (Fig. 5E,K,Q) is in the cytoplasm. Upon rapamycin treatment, the FKBP12 domain binds the FRB domain, translocating the phosphatase to the membrane (Fig. 5H,N,T). The depletion of PtdIns(4,5)P_2 results in the translocation of the PtdIns(4,5)P_2 binding partner, the PH domain of PLCδ1, from the plasma membrane to the cytoplasm (Fig. 5I). PtdIns(4,5)P_2 depletion alone does not remove F-BAR(2) from the plasma membrane (Fig. 5O), as it remains bound after rapamycin treatment. In contrast, the levels of F-BAR(3) are significantly reduced at the plasma membrane following rapamycin treatment (Fig. 5U). These results strongly argue that F-BAR(2) and F-BAR(3) display a different requirement for PtdIns(4,5)P_2 for their membrane localization, and in particular, that F-BAR(2) relies on other negatively-charged phosphoinositides or other mechanisms for its membrane localization.

F-BAR(1) constrains cellular protrusions in cortical neurons, whereas F-BAR(2) and F-BAR(3) induce protrusions

We have previously shown that the activation of full-length srGAP2 varies between COS7 cells and cortical neurons (Guerrier et al., 2009); therefore, we wanted to compare the activities of these three F-BAR domains in cortical neurons. Mouse embryos were harvested and subjected to ex utero electroporation following injection of plasmid DNA into the lateral ventricles at embryonic day 15.5 (E15.5) (for details, see Hand et al., 2005). Dorsal telencephalic progenitors were immediately dissociated and plated. At 24 hours in vitro (24 hiv), these immature neurons display high levels of lamelipodial and filopodial dynamics (Stage 1), processes that precede and are required for neurite initiation (Guerrier et al., 2009; Dent et al., 2007). The activities of the F-BAR domains of srGAPs diverge between COS7 cells and primary cortical neurons, most strikingly for srGAP1. Neurons electroporated with each of the three F-BAR domains contain more filopodia than control GFP-containing neurons (Fig. 6A–D, quantified in Fig. 6E); however, F-BAR(1) localizes very distinctly to areas of the plasma membrane that lack protrusions (arrowhead in Fig. 6B), whereas F-BAR(2) and F-BAR(3) localize to sites of filopodial and lamellipodial protrusions (Fig. 6C,D). Quantification reveals that areas of the plasma membrane where F-BAR(1) is found contains significantly less filopodia than areas of the plasma membrane that lack F-BAR(1), and vice versa for F-BAR(2) and FBAR(3) (Fig. 6F). The trend is the same for F-BAR(1) and F-BAR(2) in lamellipodial protrusions, but reversed for F-BAR(3) (Fig. 6G).

To confirm these static analyses, we performed time-lapse confocal imaging of GFP-tagged F-BAR domains co-electroporated with an F-actin probe (LifeAct-mRFPruby); (Riedl et al., 2008) into E15.5 cortical neuronal progenitors, then plated and cultured the neurons for 24 hiv (Fig. 7; supplementary material Movies 1–3). As we hypothesized, F-BAR(1) inhibits membrane protrusions and/or stabilizes the plasma membrane. Strikingly, in neurons expressing F-BAR(1)–EGFP, filopodia-like F-actin-rich protrusions were only observed where F-BAR(1) is not present (Fig. 7B–F; supplementary material Movie 1). F-BAR(2) coats the majority of the membrane, and induces the extension and retraction of neuronal F-actin-rich filopodia (Fig. 7J–R; supplementary material Movie 2); however, little to no ruffling activity occurred in the F-BAR(2)-coated membrane. F-BAR(3) appears

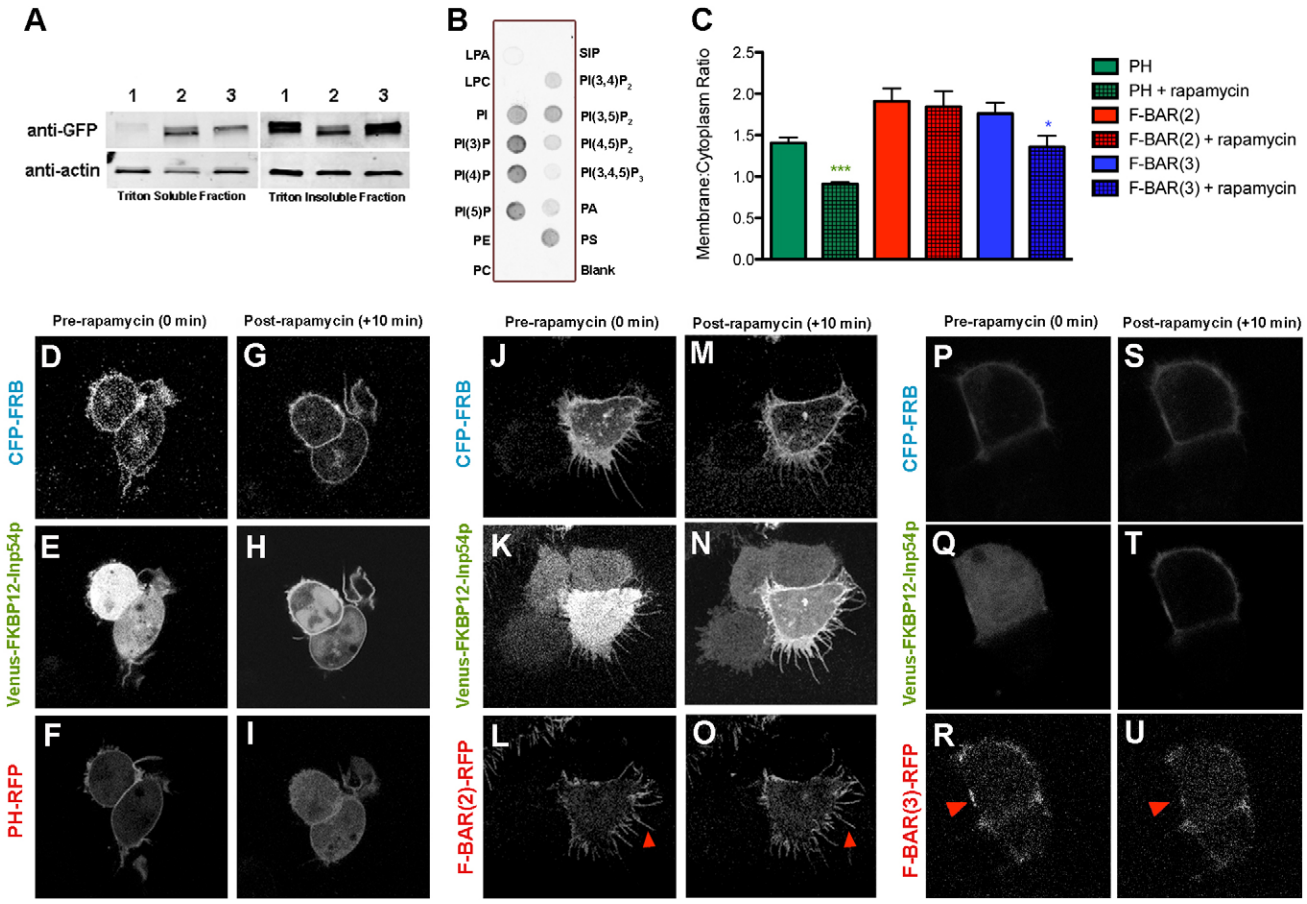

Fig. 5. F-BAR(2) binds multiple negatively-charged phospholipids. (**A**) Western blot depicting F-BARs found in two separate fractions, a Triton-X-soluble and Triton-X-insoluble fraction. The level of F-BAR(1) expression is 32-fold higher in the Triton-X-insoluble fraction, whereas the level of F-BAR(2) is slightly reduced in this fraction (0.6-fold) and F-BAR(3) is more highly expressed in the insoluble fraction (7.4-fold). (**B**) Binding of F-BAR(2) to immobilized phospholipids on nitrocellulose membrane (PIP Strip, Molecular Probes). Membrane was incubated with recombinant F-BAR(2) (amino acids 1–480) and subsequently immunoblotted with an antibody to srGAP2. LPA, lysophosphatidic acid; LPC, lysophosphatidylcholine; PE, phosphatidylethanolamine; PC, phosphatidylcholine; SIP, sphingosine 1-phosphate; PA, phosphatidic acid; PS, phosphatidylserine. (**C**) Quantification of pixel intensity of membrane to cytoplasmic localization pre- and post-rapamycin treatment (n=15–16). (**D–U**) Representative images of HEK293 cells triple-transfected with CFP–FRB, Venus–FKBP12–Inp54p, and the RFP-PH domain of PLCδ1 (D–I), F-BAR(2)–RFP (J–O), or F-BAR(3)–RFP (P–U) both pre- (C–E, I–K, P–R) and post-rapamycin treatment (F–H, L–N, S–U). Asterisks denote the difference between ratios of the pre- and post-rapamycin membrane localization to cytoplasmic localization in the same condition. *P<0.05, ***P<0.001.

to have an intermediate phenotype between F-BAR(1) and F-BAR(2) in neurons. It induces a comparable number of filopodia to F-BAR(2), yet as seen for F-BAR(1), it is more often found in areas that do not contain lamellipodia (Fig. 5D–F). Analysis of membrane dynamics reveals both filopodia protrusions and ruffling activity coinciding with F-BAR(3) expression (Fig. 7S–AA; supplementary material Movie 3). Taken together, these results demonstrate that in immature cortical neurons, F-BAR(1) restricts membrane protrusions and dynamics, whereas F-BAR(2) and F-BAR(3) domains induce filopodia protrusions through their membrane-deformation properties.

Discussion

The functional characterization of BAR-domain-containing proteins has expanded quite rapidly over the past few years. Recently, Guerrier and colleagues found that the F-BAR domain of srGAP2 shares the functional properties of I-BAR domain activity (Guerrier et al., 2009), such as those contained in IRSp53 and missing in metastasis (MIM) (Mattila et al., 2007; Millard et al., 2007; Saarikangas et al., 2009) by inducing membrane protrusions, rather than making invaginations as observed with canonical F-BAR proteins (Frost et al., 2007; Itoh et al., 2005). Recent reports (Carlson et al., 2011) and reviews (Heath and Insall, 2008) describing the subclasses of F-BAR-domain-containing proteins categorize srGAP family members into one functionally uniform subgroup; however, our work demonstrates that there are discrete roles and intricate differences between each srGAP family member.

Although the F-BAR domains of the srGAP family are all able to induce filopodia-like membrane protrusions to a greater extent than in control conditions, the degree to which these three domains induce such structures greatly varies. F-BAR(2) is much more potent at inducing protrusions than either F-BAR(1) or F-BAR(3) in COS7 cells, and F-BAR(1) actively restricts protrusive activity in cortical neurons. It is interesting to note

Journal of Cell Science

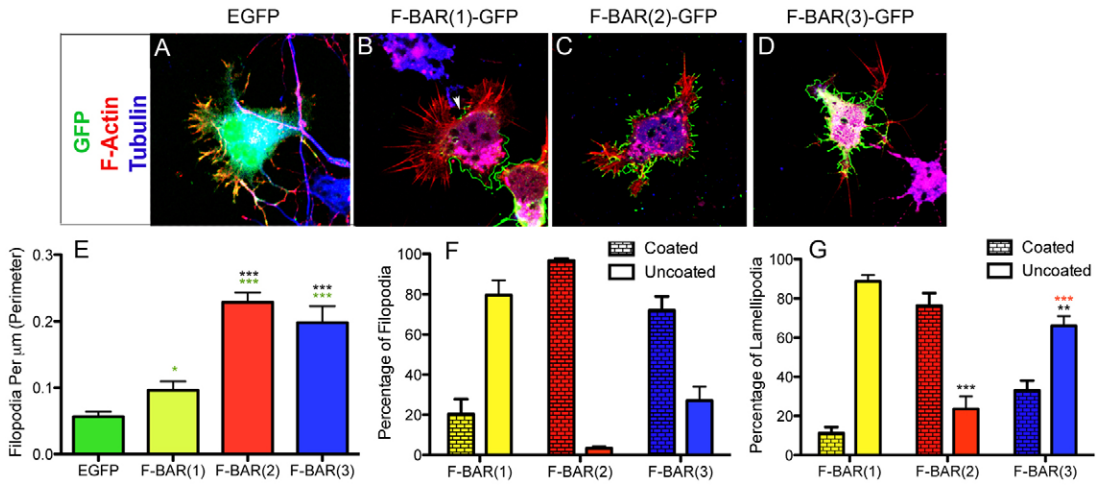

Fig. 6. F-BAR domains of srGAP proteins differ in their ability to induce filopodia in cortical neurons. (**A**–**D**) E15.5 cortical neurons expressing EGFP (A) or EGFP-tagged F-BAR(1) (B), F-BAR(2) (C), or F-BAR(3) (D) were cultured for 24 hours in vitro (hiv) after ex vivo electroporation, fixed and stained with the F-actin marker phalloidin (red). (**E**) Cells with any of the three F-BARs contain more filopodia than GFP alone, although F-BAR(2) and F-BAR(3) induce significantly more filopodia than F-BAR(1). (**F**,**G**) Quantifications of the percentage of plasma membrane in filopodia (F) or lamellipodia (G) that is coated or uncoated with F-BAR protein. Quantifications were performed on at least three independent cultures and analyzed using Mann-Whitney test (**$P<0.01$, ***$P<0.001$; $n>20$ neurons). Black asterisks illustrate comparison against F-BAR(1), whereas red asterisks indicate difference from F-BAR(2).

that COS7 cells do not express endogenous srGAP1, 2 or 3 proteins (supplementary material Fig. S1E), whereas cortical neurons express all three srGAP proteins in various combinations throughout development in vitro and in vivo (supplementary material Fig. S1G) (Bacon et al., 2009). Bacon et al. demonstrated that mRNA encoding srGAP3 appears to be the most highly expressed among srGAPs in the cortex at early developmental time points, followed closely by that of srGAP2, whereas srGAP1 is not significantly expressed until postnatal ages (Bacon et al., 2009). We find similar expression levels in dissociated cortical neurons (supplementary material Fig. S1G). Interestingly, srGAP2 protein increases within a few days in culture, whereas srGAP3 remains relatively stable. However, immunohistochemical analysis of srGAP2 and srGAP3 in cortical

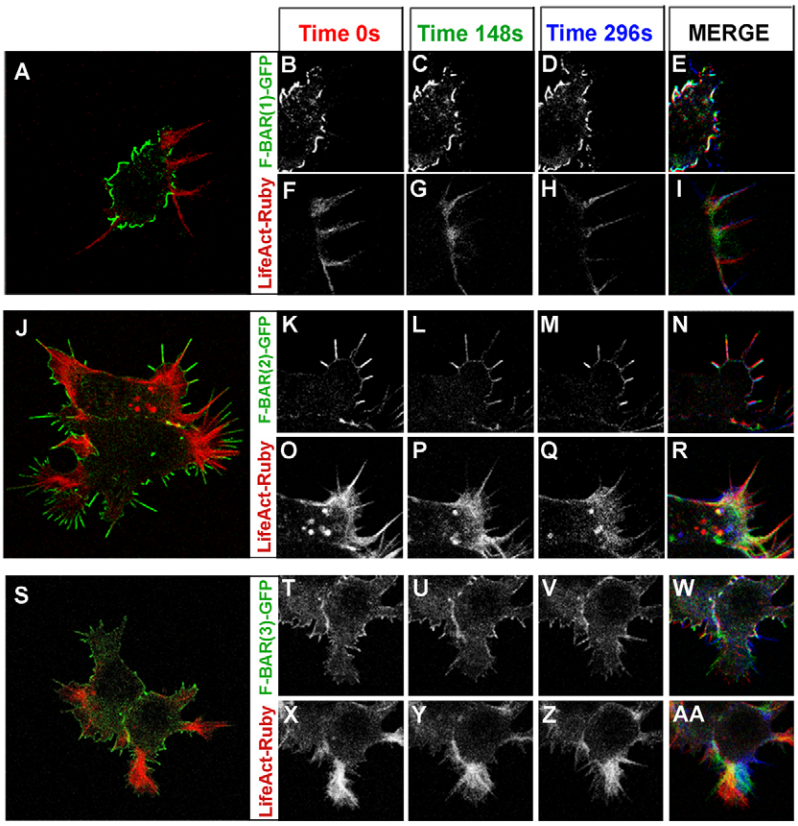

Fig. 7. Real-time imaging of membrane and F-actin dynamics induced by F-BAR domains in cortical neurons. E15.5 cortical neurons expressing the F-actin probe LifeAct-mRFPruby (red) and GFP-tagged F-BAR(1) (**A**–**I**), F-BAR(2) (**J**–**R**), or F-BAR(3) (**S**–**AA**) following ex vivo electroporation and 24 hours in dissociated culture. GFP and mRuby channels are shown separately for ease of visualization (supplementary material Movies 1–3). Images from time series taken at 0, 148 and 296 seconds are pseudocolored in red, green and blue, respectively. The white overlay in the merge panel indicates limited spatial dynamics throughout the movie. (A) Whole-cell image of a cortical neuron coexpressing F-BAR(1)–EGFP and LifeAct-mRFPruby. (B–I) F-BAR(1)-coated membrane shows little to no spatial dynamics (B–E); however, dynamic neuritic protrusions can be visualized with LifeAct-mRFPruby at sites of 'breaks' in F-BAR(1)–GFP coated plasma membrane (F–I). (J) Whole-cell image of F-BAR(2)–EGFP and LifeAct-mRFPruby co-expressing neuron. (K–R) F-BAR(2)-coated membrane displays rapid extension and retraction of filopodia protrusions (K–N), although F-actin dynamics are largely confined to the area within the F-BAR(2)-coated membrane (O–R). (S) Whole-cell image of a cortical neuron coexpressing F-BAR(3)–EGFP and LifeAct-mRFPruby. (T–AA) F-BAR(3)–GFP-coated membrane presents numerous sites of filopodia-like membrane dynamics.

Journal of Cell Science

neurons reveals no distinguishable difference in endogenous subcellular localization, with both proteins producing punctate staining throughout the cell body and protrusions (data not shown) (Guerrier et al., 2009; Endris et al., 2011). Our data argue that, upon its exogenous expression, the F-BAR domain might interact with endogenous forms of these srGAP proteins, possibly explaining the different effects of these proteins when expressed in COS7 cells vs. cortical neurons. Given the high expression of endogenous srGAP3 in cortical neurons, this interaction could particularly explain the differences seen with F-BAR(3). In addition to differential expression of srGAP proteins between COS7 cells and neurons, cortical neurons display extensive filopodia dynamics during neurite initiation (Dent et al., 2007) as well as during spine formation (Yoshihara et al., 2009), whereas COS7 cells rarely display spontaneous filopodia formation (Fig. 1A–A″). These differences in native cytoskeleton composition and dynamics, as well as variance of membrane and cytoskeletal-related proteins, might also help to explain the differences we observed between F-BAR activities in these two cell types.

Recent analysis of srGAP3 (also called WAVE-1 related protein, WRP, and MEGAP) has shown that its F-BAR domain is involved in filopodia induction preceding spine morphogenesis (Carlson et al., 2011). However, those authors suggested that the F-BAR domain of srGAP3 is targeted to the plasma membrane through its ability to bind to PtdIns(4,5)P_2 and PtdIns(3,4,5)P_3. Our analysis shows a strikingly different pattern of phospholipid binding for the F-BAR domain of srGAP2, which seems to bind very broadly to negatively charged phospholipids, including six out of seven existing phosphoinositides, as well as PtdSer. In their analysis of the binding of F-BAR(3) to the membrane, Carlson et al. (Carlson et al., 2011) used a constitutively active PtdIns(4,5)P_2 phosphatase, Inp54p, to reduce PtdIns(4,5)P_2 levels at the plasma membrane; however, constitutive Inp54p expression leads to changes in cell shape due to PtdIns(4,5)P_2-mediated alterations in the actin cytoskeleton from reduced interaction between the actin network and the plasma membrane (Raucher et al., 2000). Given the close interaction of many BAR-containing proteins with the cytoskeleton as well as with the plasma membrane, we wanted to look at the effects of acute PtdIns(4,5)P_2 depletion on F-BAR membrane-binding. Our results demonstrate that acute depletion of PtdIns(4,5)P_2 has no effect on the targeting of F-BAR(2) to the plasma membrane, however it does affect F-BAR(3) localization. We did not find coexpression alone to be effective enough to reduce localization of F-BAR(3) (data not shown); however, the difference between the ability to induce translocation upon acute, inducible PtdIns(4,5)P_2 depletion is clearly compatible with the lack of binding specificity of F-BAR(2) to PtdIns(4,5)P_2, and suggests that the F-BAR domain of srGAP2 could bind to the plasma membrane through other negatively charged phospholipids, including PtdSer. An interesting possibility exists that these proteins need the electrostatic charge interaction primarily for initial binding, and subsequently localization occurs through hydrophic interaction such as the insertion of an amphipathic helix seen in N-BAR (Itoh and De Camilli, 2006) and I-BAR domains (Saarikangas et al., 2009). While the F-BAR domain of srGAP3 does translocate after PtdIns(4,5)P_2 depletion, the effect is less specific and more variable than with the PH domain of PLCδ1. This variation, as well as the lack of translocation with F-BAR(2), could be accounted for by the broad lipid specificity, a physical insertion into the plasma membrane, or both.

Alternatively, F-BARs of the srGAP family could be tuned to differentially bind to a specific range of membrane curvature found at the plasma membrane, as previously shown for other BAR and F-BAR domains (Frost et al., 2007; Zhao et al., 2011). This could further explain the differential localization between the srGAP F-BAR domains within filopodial protrusions, where curvature varies along the base, neck and tip of a filopodium. The molecular mechanisms underlying the differences in phospholipid-binding specificity between F-BAR(2) and F-BAR(3) are currently unknown, but might involve differences in electrostatic positive charge distribution (lysine and arginine residues) at the surface of these two F-BAR dimers; however, the structures of these F-BAR domains have yet to be solved, therefore, further experiments will be necessary to identify the precise molecular basis for these differences. The molecular basis for self-assembly of this class of F-BAR domains is currently unknown, however shorter F-BAR domains present in proteins such as FBP17, have been shown to interact through both ‘end-to-end’ interactions as well as ‘side-to-side’ interactions of individual dimers. These oligomers form a corkscrew-like helix that binds and tubulates membranes (Frost et al., 2008; Shimada et al., 2007; Wang et al., 2009). Based on combinations of in vitro cryo-EM, structural and bio-informatics modeling analysis, it was found that F-BAR and I-BAR proteins are able to form molecular assemblies inducing specific membrane topologies, ranging from membrane tubules to shallow membrane curvature (Frost et al., 2008; Wang et al., 2009), and even to planar membrane sheets (Pykäläinen et al., 2011). However, the mechanisms underlying F-BAR domain assembly in cells and the way they control membrane deformation and dynamics is currently unknown, and warrants further investigation. Our data show for the first time that the F-BAR domains of srGAP proteins have different functions and dynamics in both cell lines and primary neurons. These F-BAR domains display different lipid-binding properties, as well as a clear F-actin-dependence for their intracellular mobility (supplementary material Fig. S4). Our data raise the possibility that F-BAR(1) and F-BAR(3), which have lower mobile fraction coefficients than F-BAR(2) in various conditions, could have a stronger association with the plasma membrane and therefore aid in membrane stabilization as opposed to membrane deformation. Our time-lapse data in neurons support this hypothesis by revealing that there is a reduced number of membrane protrusions where F-BAR(1) is present at the plasma membrane, as well as reduced filopodial dynamics in transfected COS7 cells. Our results also point to the fact that the F-BAR domains of three srGAP proteins are able to interact and possibly heterodimerize, and that these three F-BAR domains act synergistically towards filopodia formation (Figs 2, 3; supplementary material Fig. S4). Overall, our results point to the unique function of the srGAP family proteins, through their F-BAR domains, in inducing and regulating filopodia-like protrusions in neuronal and non-neuronal cells because of their ability to control membrane deformation.

Materials and Methods

Plasmid constructs and sequence alignments

All srGAP constructs were cloned into a modified pCIG2 vector (Guerrier et al., 2009) with the IRES removed for GFP-, RFP- or Myc-tagged C-terminal fusions. Lifeact-pRuby was subcloned from EGFP-N1 into the modified pCIG2 construct, using XhoI/NotI cut sites. srGAP constructs contain the following proteins and

Journal of Cell Science

F-BAR truncations: human full-length srGAP1 (GenBank number NP_065813.1), srGAP2 (GenBank number NP_056141.2), srGAP3 (GenBank number NP_001028289.1), or F-BAR truncations F-BAR(1) (aa 1–516), F-BAR(2) (aa 1–501), F-BAR(3) (aa 1–492). Constructs for rapamycin-induced PtdIns(4,5)P_2 depletion, with the exception of F-BAR(2)–RFP and F-BAR(3)–RFP described above, were obtained from Tamas Balla (NICHD, Bethesda, MD) and Tobias Meyer (Stanford, Stanford, CA) and cloned into pcDNA3.1 by Sam Snider (Zylka Lab, UNC-Chapel Hill, NC). Protein phylogenetic tree prediction was created using GeneBee TreeTop (http://www.genebee.msu.su/). The percentage of amino acid conservation was determined with the NCBI Blast tool. Sequence alignments were created using MultAlign (Corpet, 1988).

Cell culture

COS7 and HEK293 cells were plated onto poly-D-lysine-coated coverslips (Sigma P0899) and maintained in Dulbecco's Modified Eagle's Medium (DMEM, Sigma D6046) supplemented with 10% FBS (Foundation 900-108) and 1× Penicillin-Streptomycin (Pen/Strep, Gibco 15070-063). Cell culture transfections were performed 24 hours post plating, using Lipofectamine 2000 (Invitrogen 11668) according to the manufacturer's instructions. Fixed cells were treated with 4% paraformaldehyde for 20 minutes, washed in PBS, permeabilized in 0.05% Triton X-100 in PBS, washed, and then blocked in 5% BSA (Sigma A6003) for 20 minutes. COS7 cells were then incubated with primary antibody (anti-myc antibody 1:500, Cell Signaling 2276; anti-GFP antibody 1:1000, Aves GFP-1020; or anti-RFP antibody 1:1000, Invitrogen R10367) in PBS with 0.2% BSA and 10% normal goat serum overnight at 4℃. Cells were washed in PBS and incubated with secondary antibody [goat anti-chicken Alexa-Fluor-488 (1:1000, Invitrogen A11039), goat anti-rabbit Alexa-Fluor-546 (1:1000, Invitrogen A11035), Alexa-Fluor-546–phalloidin (1:200, Invitrogen A22283), Alexa-Fluor-647 phalloidin (1:200, Invitrogen A22287), or DRAQ5 (1:10,000, Fisher NC9165029)] for 2 hours at room temperature. Finally, cells were then washed in PBS and mounted with Biomedia mounting media (Fisher NC9034735).

Primary neuronal cultures were plated onto poly-D-lysine- or laminin-coated coverslips (Sigma L2020) and maintained for 24 hours in Neurobasal-A (Invitrogen 10888-022) supplemented with 1× Pen/Strep, L-glutamine (Gibco 25030-081), 1× B-27 (Gibco 17504044) and N2 (Gemini 400-163). Cortical neurons were transfected prior to dissociation via ex vivo electroporation at E15.5, as previously described (Hand et al., 2005). Neurons were fixed for 10 minutes at 24 hours after plating, using a 1% glutaraldehyde solution in PHEM buffer (pH 6.9; 60 mM PIPES, 25 mM HEPES, 10 mM EGTA, and 2 mM $MgCl_2$) to preserve cytoskeletal integrity (Kaech et al., 1997). The rest of the staining protocol is the same as used for COS7 cells, with the primary antibodies anti-GFP (Invitrogen A11122) and anti-tubulin (Covance MMS-435P-100), and secondary antibodies goat anti-rabbit Alexa-Fluor-488 (Invitrogen 11034), Alexa-Fluor-546 phalloidin and goat anti-mouse Alexa-Fluor-647 (Invitrogen A21235).

To determine filopodia number, fixed cells were imaged using LEICA TCS SL confocal microscope, with a 63×/1.4NA oil immersion objective. Magnified images (×2) were taken of representative cells from each construct. Images were then imported to NIH ImageJ. Using the line tool, a perimeter was drawn around the cells. The presence of filopodia was determined by counting the number of consecutive pixels on the line drawn around the cell perimeter and normalized by dividing the total number of filopodia by the cell perimeter (filopodia per μm). Protein extension into filopodia was determined using NIH ImageJ software to draw a line from the base to the tip of the filopodium, and measure fluorescence intensity of each fluorescence channel.

Live-cell imaging

Live cell imaging of COS7 cells, HEK293 cells, and neuronal cultures were imaged using Leica TCS confocal microscope with either a 20× objective, or a 63×/1.4NA oil immersion objective, with a 37℃ stage warmer. COS7 cells were imaged in their culture medium at 12-second intervals. The path of filopodial tips was traced over time using NIH ImageJ software to obtain quantification of filopodial dynamics (μm/minute). Culture medium was removed from HEK cells prior to imaging, and replaced with 37℃ Hank's Balanced Salt Solution (HBSS, Gibco 14025) supplemented with 0.24% HEPES (Fisher BP310), 0.2% dextrose (Fisher D16) and 0.1% BSA (Sigma A6003). Images were taken before and after addition of 1 μM rapamycin (Calbiochem 553212) in supplemented HBSS solution was added to the cells. Membrane to cytoplasm ratio in pre- and post-ramapycin-treated cells was measured in HEK cells expressing all three constructs, using NIH ImageJ software. Neuronal cultures were imaged in their culture medium, at 12-second intervals.

Live-cell imaging for FRAP experiments was performed with a PLAPO 60×/1.42 objective (Olympus) on an Olympus FV1000 confocal microscope, equipped with a plastic cage incubator (Presicion Plastics, MA) maintained at 37℃ with 5% CO_2 and 60% humidity to prevent media evaporation. To measure fast fluorescence dynamics in single filopodia images of 256×256 pixels were taken at 36× zoom with pixel dwell time of 2 μs. A rectangular shape bleach area of a fixed width (~0.4 μm) was drawn across the filopodia or a membrane region, 20 prebleach frames acquired with a 488 excitation laser (multiline Argon laser) attenuated to 0.7% to minimize photobleaching of the sample, followed by 300 ms bleaching with the same laser operated at full power. The recovery was then measured at the speed of ~0.5 seconds/frame with the 488 laser, operated at the same 0.7% transmission as for the prebleaching acquisition. For cytochalasin-D treatments, COS7 cells were transfected with F-BAR constructs and cultured for 48 hours. Cells were then treated with 200 μM cytochalasin D (Sigma C2873) for 1 hour prior to imaging. To observe the presence of F-actin, cells were fixed post-imaging and stained with phalloidin as previously stated. Fluorescence intensity curve from FRAP imaging was then analyzed with the Igor Pro 6.12A (Wavemetrics) using the K_FRAPcalc v9 procedure developed by Kota Miura (EMBL).

Biochemistry

Western blots were run from COS7 cells transfected with either tagged F-BAR, or full-length srGAP constructs, treated with Ripa Buffer (50 mM Tris, pH 7.4, 1% Triton X-100, 0.25% sodium deoxycholate, 0.1% SDS, 1 mM EDTA, 150 mM NaCl, 1× Complete Protease Inhibitor Cocktail (Roche), 1 mM PMSF) at 24 hours post transfection. Lysates were run through 4–12% NuPage gels (Invitrogen NP0321) and transferred onto a PVDF membrane (Amersham RPN303F), which was then blocked with 5% dry milk (Carnation) in TBS-T. Primary antibodies (anti-srGAP1 1:1000, Abcam ab57504; anti-srGAP2 A2 and anti-srGAP3 A1 1:1000; gifts from Wei-Lin Jin lab, University of Shangai; anti-GFP 1:1000, Invitrogen A11122; and anti-Actin 1:5000, Millipore MAB 1501) and secondary antibodies (donkey anti-rabbit IRDye 800, Li-cor Biosciences 926-32213; or donkey anti-mouse IRDye 680, Licor Biosciences 926-32222) were incubated in 3% dry milk in TBS-T.

Co-immunoprecipitations were obtained from double-transfected cells and treated with co-immunoprecipitation buffer (50 mM Tris-HCl pH 7.4, 15 mM EGTA, 100 mM NaCl, 0.1% Triton X-100, protease inhibitor, 1 mM DTT and 1 mM PMSF) 24 hours after transfection. Incubations and washes were performed in the same buffer. 10% of the lysis volume was collected prior to antibody incubations for input controls. The rest of the co-immunoprecipitation lysis was subjected to the immunoprecipitation antibody (1 μg anti-GFP, Invitrogen A11122, or 1 μg anti-IgG control antibody) bound to Protein A/G beads (Santa Cruz 2003), washed and dissociated with SDS loading buffer at 95℃. The two-step lysis buffer, to analyze Triton-X-soluble and Triton-X-insoluble fractions, was first subjected to the co-immunoprecipitation buffer described above. The lysates were then centrifuged at 25,200 ***g*** for 20 minutes. The supernatent was removed and used for the Triton-X-soluble fraction. The insoluble pellet was then subjected to a modified RIPA buffer (50 mM Tris-HCl pH 7.4, 0.5% sodium deoxycholate, 0.2% SDS, 1 mM EDTA, 150 mM NaCl, 1mM PMSF and 1× protease inhibitor), sonicated briefly and spun at 25,200 ***g*** for 10 minutes. The supernatent was removed and used for the Triton-X-insoluble fraction. Western blots were run as described before, using anti-GFP, anti-RFP or anti-Myc primary antibodies, and anti-mouse and anti-rabbit antibodies described above. Western blots were imaged on the LI-COR Odyssey infrared imaging system.

Immobilized lipids were spotted onto PIP Strip membranes (Molecular Probes P23750) and treated according to manufacturer's instructions. Briefly, the PIP Strip membrane was blocked with 3% BSA/TBS-T (Sigma A6003), incubated with 0.5 μg/ml purified F-BAR(2) (aa 1–480; purified by the laboratory of Holger Sondermann, Cornell University, Ithaca, NY) in 3% BSA/TBS-T for 1 hour at room temperature, washed in TBS-T, incubated with primary antibody (anti-srGAP2 A1 1:1000; a gift from Wei Lin Jin, Shanghai Univ., China), washed in TBS-T, incubated with secondary antibody (goat anti-rabbit IRDye800), washed, and developed using the LI-COR Odyssey infrared imaging system.

Acknowledgements

The authors thank Tobias Meyer and Tamas Balla for supplying the constructs used in the phosphatase translocation experiment, as well as Sam Snider for additional cloning of these constructs. We thank Takayuki Sassa for cloning the srGAP1 and F-BAR(1) constructs used in this study, Wei Lin Jin for srGAP2 and srGAP3 antibodies, Kota Miura for valuable discussions about FRAP analysis, Joe Rittiner for providing HEK cells, Sabrice Guerrier for scientific advice and discussion.

Funding

This research was supported by the National Institutes of Health [grant numbers 1F31NS068038 to J.C.B., 5P30NS045892 to V.G., 7R01NS067557 to F.P.]; and an anonymous donor (to M.J.Z.). Deposited in PMC for release after 12 months.

Supplementary material available online at
http://jcs.biologists.org/lookup/suppl/doi:10.1242/jcs.098962/-/DC1

Journal of Cell Science

References

Bacon, C., Endris, V. and Rappold, G. (2009). Dynamic expression of the Slit-Robo GTPase activating protein genes during development of the murine nervous system. *J. Comp. Neurol.* **513**, 224-236.

Carlson, B. and Soderling, S. H. (2009). Mechanisms of cellular protrusions branch out. *Dev. Cell* **17**, 307-309.

Carlson, B. R., Lloyd, K. E., Kruszewski, A., Kim, I. H., Rodriguiz, R. M., Heindel, C., Faytell, M., Dudek, S. M., Wetsel, W. C. and Soderling, S. H. (2011). WRP/srGAP3 facilitates the initiation of spine development by an inverse F-BAR domain, and its loss impairs long-term memory. *J. Neurosci.* **31**, 2447-2460.

Corpet, F. (1988). Multiple sequence alignment with hierarchical clustering. *Nucleic Acids Res.* **16**, 10881-10890.

Dent, E. W., Kwiatkowski, A. V., Mebane, L. M., Philippar, U., Barzik, M., Rubinson, D. A., Gupton, S., Van Veen, J. E., Furman, C., Zhang, J. et al. (2007). Filopodia are required for cortical neurite initiation. *Nat. Cell Biol.* **9**, 1347-1359.

Dharmalingam, E., Haeckel, A., Pinyol, R., Schwintzer, L., Koch, D., Kessels, M. M. and Qualmann, B. (2009). F-BAR proteins of the syndapin family shape the plasma membrane and are crucial for neuromorphogenesis. *J. Neurosci.* **29**, 13315-13327.

Doherty, G. J. and McMahon, H. T. (2008). Mediation, modulation, and consequences of membrane-cytoskeleton interactions. *Annu. Rev. Biophys.* **37**, 65-95.

Endris, V., Wogatzky, B., Leimer, U., Bartsch, D., Zatyka, M., Latif, F., Maher, E. R., Tariverdian, G., Kirsch, S., Karch, D. et al. (2002). The novel Rho-GTPase activating gene MEGAP/ srGAP3 has a putative role in severe mental retardation. *Proc. Natl. Acad. Sci. USA* **99**, 11754-11759.

Endris, V., Haussmann, L., Buss, E., Bacon, C., Bartsch, D. and Rappold, G. (2011). SrGAP3 interacts with lamellipodin at the cell membrane and regulates Rac-dependent cellular protrusions. *J. Cell Sci.* **124**, 3941-3955.

Flesch, F. M., Yu, J. W., Lemmon, M. A. and Burger, K. N. (2005). Membrane activity of the phospholipase C-delta1 pleckstrin homology (PH) domain. *Biochem. J.* **389**, 435-441.

Foletta, V. C., Brown, F. D. and Young, W. S., 3rd (2002). Cloning of rat ARHGAP4/C1, a RhoGAP family member expressed in the nervous system that colocalizes with the Golgi complex and microtubules. *Brain Res. Mol. Brain Res.* **107**, 65-79.

Ford, M. G., Mills, I. G., Peter, B. J., Vallis, Y., Praefcke, G. J., Evans, P. R. and McMahon, H. T. (2002). Curvature of clathrin-coated pits driven by epsin. *Nature* **419**, 361-366.

Frost, A., De Camilli, P. and Unger, V. M. (2007). F-BAR proteins join the BAR family fold. *Structure* **15**, 751-753.

Frost, A., Perera, R., Roux, A., Spasov, K., Destaing, O., Egelman, E. H., De Camilli, P. and Unger, V. M. (2008). Structural basis of membrane invagination by F-BAR domains. *Cell* **132**, 807-817.

Guerrier, S., Coutinho-Budd, J., Sassa, T., Gresset, A., Jordan, N. V., Chen, K., Jin, W. L., Frost, A. and Polleux, F. (2009). The F-BAR domain of srGAP2 induces membrane protrusions required for neuronal migration and morphogenesis. *Cell* **138**, 990-1004.

Han, J. W., Leeper, L., Rivero, F. and Chung, C. Y. (2006). Role of RacC for the regulation of WASP and phosphatidylinositol 3-kinase during chemotaxis of Dictyostelium. *J. Biol. Chem.* **281**, 35224-35234.

Hand, R., Bortone, D., Mattar, P., Nguyen, L., Heng, J. I., Guerrier, S., Boutt, E., Peters, E., Barnes, A. P., Parras, C. et al. (2005). Phosphorylation of Neurogenin2 specifies the migration properties and the dendritic morphology of pyramidal neurons in the neocortex. *Neuron* **48**, 45-62.

Harlan, J. E., Hajduk, P. J., Yoon, H. S. and Fesik, S. W. (1994). Pleckstrin homology domains bind to phosphatidylinositol-4,5-bisphosphate. *Nature* **371**, 168-170.

Heath, R. and Insall, R. (2008). F-BAR domains: multifunctional regulators of membrane curvature. *J. Cell Sci.* **121**, 1951-1954.

Henne, W. M., Kent, H. M., Ford, M. G., Hegde, B. G., Daumke, O., Butler, P. J., Mittal, R., Langen, R., Evans, P. R. and McMahon, H. T. (2007). Structure and analysis of FCHo2 F-BAR domain: a dimerizing and membrane recruitment module that effects membrane curvature. *Structure* **15**, 839-852.

Itoh, T. and De Camilli, P. (2006). BAR, F-BAR (EFC) and ENTH/ANTH domains in the regulation of membrane-cytosol interfaces and membrane curvature. *Biochim. Biophys. Acta* **1761**, 897-912.

Itoh, T., Erdmann, K. S., Roux, A., Habermann, B., Werner, H. and De Camilli, P. (2005). Dynamin and the actin cytoskeleton cooperatively regulate plasma membrane invagination by BAR and F-BAR proteins. *Dev. Cell* **9**, 791-804.

Janetopoulos, C., Borleis, J., Vazquez, F., Iijima, M. and Devreotes, P. (2005). Temporal and spatial regulation of phosphoinositide signaling mediates cytokinesis. *Dev. Cell* **8**, 467-477.

Kaech, S., Fischer, M., Doll, T. and Matus, A. (1997). Isoform specificity in the relationship of actin to dendritic spines. *J. Neurosci.* **17**, 9565-9572.

Lee, S. H., Kerff, F., Chereau, D., Ferron, F., Klug, A. and Dominguez, R. (2007). Structural basis for the actin-binding function of missing-in-metastasis. *Structure* **15**, 145-155.

London, E. and Brown, D. A. (2000). Insolubility of lipids in Triton X-100: physical origin and relationship to sphingolipid/cholesterol membrane domains (rafts). *Biochim. Biophys. Acta* **1508**, 182-195.

Martin-Belmonte, F., Gassama, A., Datta, A., Yu, W., Rescher, U., Gerke, V. and Mostov, K. (2007). PTEN-mediated apical segregation of phosphoinositides controls epithelial morphogenesis through Cdc42. *Cell* **128**, 383-397.

Masuda, M., Takeda, S., Sone, M., Ohki, T., Mori, H., Kamioka, Y. and Mochizuki, N. (2006). Endophilin BAR domain drives membrane curvature by two newly identified structure-based mechanisms. *EMBO J.* **25**, 2889-2897.

Mattila, P. K., Pykäläinen, A., Saarikangas, J., Paavilainen, V. O., Vihinen, H., Jokitalo, E. and Lappalainen, P. (2007). Missing-in-metastasis and IRSp53 deform PI(4,5)P2-rich membranes by an inverse BAR domain-like mechanism. *J. Cell Biol.* **176**, 953-964.

Miki, H., Miura, K. and Takenawa, T. (1996). N-WASP, a novel actin-depolymerizing protein, regulates the cortical cytoskeletal rearrangement in a PIP2-dependent manner downstream of tyrosine kinases. *EMBO J.* **15**, 5326-5335.

Millard, T. H., Bompard, G., Heung, M. Y., Dafforn, T. R., Scott, D. J., Machesky, L. M. and Fütterer, K. (2005). Structural basis of filopodia formation induced by the IRSp53/MIM homology domain of human IRSp53. *EMBO J.* **24**, 240-250.

Millard, T. H., Dawson, J. and Machesky, L. M. (2007). Characterisation of IRTKS, a novel IRSp53/MIM family actin regulator with distinct filament bundling properties. *J. Cell Sci.* **120**, 1663-1672.

Mitchell, K. T., Ferrell, J. E., Jr and Huestis, W. H. (1986). Separation of phosphoinositides and other phospholipids by two-dimensional thin-layer chromatography. *Anal. Biochem.* **158**, 447-453.

Oikawa, T., Yamaguchi, H., Itoh, T., Kato, M., Ijuin, T., Yamazaki, D., Suetsugu, S. and Takenawa, T. (2004). PtdIns(3,4,5)P3 binding is necessary for WAVE2-induced formation of lamellipodia. *Nat. Cell Biol.* **6**, 420-426.

Peter, B. J., Kent, H. M., Mills, I. G., Vallis, Y., Butler, P. J., Evans, P. R. and McMahon, H. T. (2004). BAR domains as sensors of membrane curvature: the amphiphysin BAR structure. *Science* **303**, 495-499.

Pykäläinen, A., Boczkowska, M., Zhao, H., Saarikangas, J., Rebowski, G., Jansen, M., Hakanen, J., Koskela, E. V., Peränen, J., Vihinen, H. et al. (2011). Pinkbar is an epithelial-specific BAR domain protein that generates planar membrane structures. *Nat. Struct. Mol. Biol.* **18**, 902-907.

Raucher, D., Stauffer, T., Chen, W., Shen, K., Guo, S., York, J. D., Sheetz, M. P. and Meyer, T. (2000). Phosphatidylinositol 4,5-bisphosphate functions as a second messenger that regulates cytoskeleton-plasma membrane adhesion. *Cell* **100**, 221-228.

Riedl, J., A. H., Kessenbrock, K., Yu, J. H., Neukirchen, D., Bista, M., Bradke, F., Jenne, D., Holak, T. A., Werb, Z. et al. (2008). Lifeact: a versatile marker to visualize F-actin. *Nat. Methods* **5**, 605-607.

Rouquette-Jazdanian, A. K., Pelassy, C., Breittmayer, J.-P., Cousin, J.-L. and Aussel, C. (2002). Metabolic labelling of membrane microdomains/rafts in Jurkat cells indicates the presence of glycerophospholipids implicated in signal transduction by the CD3 T-cell receptor. *Biochem. J.* **363**, 645-655.

Saarikangas, J., Zhao, H., Pykäläinen, A., Laurinmäki, P., Mattila, P. K., Kinnunen, P. K., Butcher, S. J. and Lappalainen, P. (2009). Molecular mechanisms of membrane deformation by I-BAR domain proteins. *Curr. Biol.* **19**, 95-107.

Saitsu, H., Osaka, H., Sugiyama, S., Kurosawa, K., Mizuguchi, T., Nishiyama, K., Nishiumra, A., Tsurusaki, Y., Doi, H., Miyake, N. et al. (2011). Early infantile epileptic encephalopathy associated with the disrupted gene encoding Slit-Robo Rho GTPase activating protein 2 (SRGAP2). *Am. J. Med. Genet. A* **158A**, 199-205.

Sheetz, M. P. and Dai, J. (1996). Modulation of membrane dynamics and cell motility by membrane tension. *Trends Cell Biol.* **6**, 85-89.

Shimada, A., Niwa, H., Tsujita, K., Suetsugu, S., Nitta, K., Hanawa-Suetsugu, K., Akasaka, R., Nishino, Y., Toyama, M., Chen, L. et al. (2007). Curved EFC/F-BAR-domain dimers are joined end to end into a filament for membrane invagination in endocytosis. *Cell* **129**, 761-772.

Soderling, S. H., Binns, K. L., Wayman, G. A., Davee, S. M., Ong, S. H., Pawson, T. and Scott, J. D. (2002). The WRP component of the WAVE-1 complex attenuates Rac-mediated signalling. *Nat. Cell Biol.* **4**, 970-975.

Suetsugu, S., Murayama, K., Sakamoto, A., Hanawa-Suetsugu, K., Seto, A., Oikawa, T., Mishima, C., Shirouzu, M., Takenawa, T. and Yokoyama, S. (2006). The RAC binding domain/IRSp53-MIM homology domain of IRSp53 induces RAC-dependent membrane deformation. *J. Biol. Chem.* **281**, 35347-35358.

Tran, D., Gascard, P., Berthon, B., Fukami, K., Takenawa, T., Giraud, F. and Claret, M. (1993). Cellular distribution of polyphosphoinositides in rat hepatocytes. *Cell. Signal.* **5**, 565-581.

Tsujita, K., Suetsugu, S., Sasaki, N., Furutani, M., Oikawa, T. and Takenawa, T. (2006). Coordination between the actin cytoskeleton and membrane deformation by a novel membrane tubulation domain of PCH proteins is involved in endocytosis. *J. Cell Biol.* **172**, 269-279.

Vallis, Y., Wigge, P., Marks, B., Evans, P. R. and McMahon, H. T. (1999). Importance of the pleckstrin homology domain of dynamin in clathrin-mediated endocytosis. *Curr. Biol.* **9**, 257-263.

Varnai, P., Thyagarajan, B., Rohacs, T. and Balla, T. (2006). Rapidly inducible changes in phosphatidylinositol 4,5-bisphosphate levels influence multiple regulatory functions of the lipid in intact living cells. *J. Cell Biol.* **175**, 377-382.

Vogt, D. L., Gray, C. D., Young, W. S., 3rd, Orellana, S. A. and Malouf, A. T. (2007). ARHGAP4 is a novel RhoGAP that mediates inhibition of cell motility and axon outgrowth. *Mol. Cell. Neurosci.* **36**, 332-342.

Wang, Q., Navarro, M. V., Peng, G., Molinelli, E., Goh, S. L., Judson, B. L., Rajashankar, K. R. and Sondermann, H. (2009). Molecular mechanism of membrane constriction and tubulation mediated by the F-BAR protein Pacsin/Syndapin. *Proc. Natl. Acad. Sci. USA* **106**, 12700-12705.

Wong, K., Ren, X. R., Huang, Y. Z., Xie, Y., Liu, G., Saito, H., Tang, H., Wen, L., Brady-Kalnay, S. M., Mei, L. et al. (2001). Signal transduction in neuronal migration: roles of GTPase activating proteins and the small GTPase Cdc42 in the Slit-Robo pathway. *Cell* **107**, 209-221.

Yamagishi, A., Masuda, M., Ohki, T., Onishi, H. and Mochizuki, N. (2004). A novel actin bundling/filopodium-forming domain conserved in insulin receptor tyrosine kinase substrate p53 and missing in metastasis protein. *J. Biol. Chem.* **279**, 14929-14936.

Yang, Y., Marcello, M., Endris, V., Saffrich, R., Fischer, R., Trendelenburg, M. F., Sprengel, R. and Rappold, G. (2006). MEGAP impedes cell migration via regulating actin and microtubule dynamics and focal complex formation. *Exp. Cell Res.* **312**, 2379-2393.

Yoshida, S., Bartolini, S. and Pellman, D. (2009). Mechanisms for concentrating Rho1 during cytokinesis. *Genes Dev.* **23**, 810-823.

Yoshihara, Y., De Roo, M. and Muller, D. (2009). Dendritic spine formation and stabilization. *Curr. Opin. Neurobiol.* **19**, 146-153.

Zaidel-Bar, R., Joyce, M. J., Lynch, A. M., Witte, K., Audhya, A. and Hardin, J. (2010). The F-BAR domain of SRGP-1 facilitates cell-cell adhesion during C. elegans morphogenesis. *J. Cell Biol.* **191**, 761-769.

Zhao, H., Hakala, M. and Lappalainen, P. (2010). ADF/cofilin binds phosphoinositides in a multivalent manner to act as a PIP(2)-density sensor. *Biophys. J.* **98**, 2327-2336.

Zhao, H., Pykäläinen, A. and Lappalainen, P. (2011). I-BAR domain proteins: linking actin and plasma membrane dynamics. *Curr. Opin. Cell Biol.* **23**, 14-21.

Journal of Cell Science